SCIENTIFIC Publishing Limited

New Energy Exploitation and Application

http://ojs.ukscip.com/journals/neea

Article

Techno-Economic Analysis of Heat-Assisted Hydrogen Production from Nuclear Power

Christopher Connolly [*], Kate Taylor, Mark Bankhead, Richard Jarvis and Jason Dean

National Nuclear Laboratory, Sellafield, Seascale, Cumbria CA20 1PG, UK
[*] Correspondence: christopher.connolly@uknnl.com

Received: 12 March 2024; **Revised**: 13 April 2024; **Accepted**: 22 April 2024; **Published**: 30 April 2024

Abstract: To play a full role in decarbonisation, hydrogen must be produced economically at scale; the role of nuclear power is interesting to national governments as it is capable of supplying both low-carbon electricity and high-quality heat. Depending on the hydrogen production technology choice, a plant may require electricity and/or heat input. This techno-economic evaluation considers not only the costs of the hydrogen plant itself but also the costs of the power supply it requires. This paper calculates cost estimates for *HTSE* (High Temperature Steam Electrolysis) coupled with nuclear heat and electricity, and a thermochemical *SI* (Sulphur Iodine) cycle coupled with nuclear heat, based on the predictions of technical process models. These estimates are then compared to estimates made elsewhere for the costs of using wind with low temperature liquid water electrolysis, and steam methane reformation with carbon capture. This analysis led to the identification of the conditions under which nuclear-heat-coupled hydrogen production would be competitively priced. Estimates for nuclear-coupled $LCOH_2$ (levelised cost of hydrogen) in 2050 range from 2.14 to 1.24 £/kg for *HTSE*, and from 2.88 to 0.89 £/kg for the *SI* cycle. There is still a great deal of uncertainty around the efficiency of *SI* and how it may improve over time, and this limits the accuracy to which the $LCOH_2$ can be predicted.

Keywords: nuclear; hydrogen; production; economics; technology readiness levels; steam electrolysis; thermochemical

1. Introduction

Hydrogen is expected to play a major role in decarbonisation due to its potential as a low carbon fuel and as a chemical feedstock for sustainable liquid fuels and products [1], while nuclear power is poised to drive hydrogen production technologies with a stable supply of low carbon electricity and heat at the gigawatt scale [2,3]. There are a range of hydrogen generation technologies currently being deployed. Alkaline electrolysis, and PEM (polymer electrolyte membrane) electrolysis are at a high technology readiness level (TRL) and are already being deployed with nuclear on MW scales [4]; these technologies are mature and only require input electricity to produce hydrogen from liquid water.

With an input of heat as well as electricity, high temperature steam electrolysis (*HTSE*) can be conducted with solid oxide cells; *HTSE* allows for a large efficiency increase versus the lower temperature electrolysis of liquid water, and is due to be demonstrated on the MW scale, coupled to a nuclear reactor, between 2023–2025 as part of the Bay Hydrogen Hub in the UK [5]. Worldwide, nuclear-coupled high temperature electrolysis is reaching high technology readiness levels (7 and above), as several commercial-scale demonstrators are due to become operational in 2024–2025 [6].

Thermochemical hydrogen generation methods offer the opportunity to utilise heat exclusively, and do not require electricity to directly drive the reaction. However, they do require high temperatures, and are in earlier stages of development than electrolysis technologies.

The levelised cost of hydrogen ($LCOH_2$) is widely used as a measure to compare the costs of different hydrogen production technologies [7]. The inclusion of heat as an energy vector has the potential to make a significant difference to the $LCOH_2$. However, not all energy sources are equally suited to producing heat at scale. In the case of most renewables, electricity would have to first be converted to heat to reach these temperatures, and of course, all energy transfers incur some energy loss. However, nuclear fission primarily produces heat, which is usually then used to convert water into steam to drive a turbine and create electricity. Depending on the technology choice, the efficiency of converting from nuclear heat to electricity is around 33–50% [8]. Utilising nuclear heat directly, then, could therefore be significantly cheaper than nuclear electricity per kW, due to two main factors:

- As previously discussed, heat is understood to make some hydrogen generation processes more efficient, and high temperature heat is an essential prerequisite for the thermochemical processes (should they prove cheaper or more efficient than other technologies in the longer term they will need a reliable heat source to scale up);
- A not insignificant percentage of the $LCOH_2$ is estimated to be due to the cost of the input energy, as opposed to the OPEX (operational expenditure) and CAPEX (capital expenditure) [9] of a hydrogen generation plant. If cost savings can be made by using a cheap source of heat energy as opposed to electricity, this has the potential to dramatically affect the overall cost per unit of hydrogen.

Nuclear energy has a further advantage. Some heat can be siphoned off from existing or future nuclear plants without significantly affecting the performance of the reactor (diverting lower grade heat from the low pressure turbines in the secondary steam cycle) so they may continue to generate the majority of their rated electricity output.

2. Materials and Methods

2.1. Technoeconomic Models

Technoeconomic models are a useful means to evaluate the cost-benefit of different energy generation systems. In general, they calculate the cost profile of a project throughout its lifetime and weigh this against the energy production profile. As such, they can help identify the optimal technology choice for new energy generation projects. The purpose of the technoeconomic assessment performed here is to estimate the opportunity for nuclear power to contribute to hydrogen production, primarily in the UK.

Renewable sources will contribute their share to the production of hydrogen, but the scale of demand (across sustainable fuels, grid balancing, and heating applications) is anticipated to rise rapidly over the next 25 years [10]. Nuclear power plants are a reliable source of low-carbon energy with a high-capacity factor, in the form of electricity and/or heat. This offers advantages in terms of the reliability of the supply of energy to a hydrogen generation plant (*HGP*), which can be important when trying to justify the CAPEX costs of an *HGP*. Whilst some renewable systems have explored the production of heat (such as concentrated solar thermal technology [11]), the benefits of this have not yet been fully realised. To be a serious option for powering hydrogen generation, nuclear technologies must also be cost-competitive with renewables and fossil fuels with carbon capture. These are the questions to be explored in this paper.

There are existing economic overviews [12–14] as well as numerous technoeconomic models for hydrogen production, including: HEEP (Hydrogen Economic Evaluation Program) [8], H2A (H2 Analysis) [15], and G4ECONS (Generation IV spreadsheet calculation of nuclear systems) [16]; but the user often has little visibility of the proprietary calculations undertaken in between. Other technoeconomic models of nuclear hydrogen production such as [17] in particular, as well as [18–20], and [21] (which considers carbon capture alongside cogeneration) go into extensive depth. The model described in this paper was developed to allow for independent assessment of the efficacy of nuclear hydrogen with a tool that can be updated and added to in future work. It is built modularly to allow for a mix-and-match selection of reactors and hydrogen production technologies. Its underlying assumptions are based on mechanistically based process models, allowing for future

improvements as more R&D and real-world performance data become available. These models pass data to a technoeconomic model from which the $LCOH_2$ is calculated.

2.2. The Technoeconomic Model

$LCOH_2$ is defined as the cost per unit that the hydrogen would have to be sold to cover the costs of generation (the 'break even' point) according to Equation (1):

$$LCOH_2 = storage\ costs + transport\ costs + energy\ source\ costs + hydrogen\ plant\ costs \quad (1)$$

The transport and storage costs are not accounted for in the model, this is an important omission however this is in line with many other models. None of the counterfactuals explored later in this paper include hydrogen storage and transport costs in $LCOH_2$. As multiple suppliers are likely to share similar storage and transport infrastructure, these are not the factors that are expected to cause significant differences in $LCOH_2$ based on hydrogen generation and energy source technology choices. The literature suggests that 5–10% is a reasonable estimate for the contribution of transport and storage costs to nuclear $LCOH_2$ [9]. Intermittent power sources, such as renewables, may incur greater storage costs as greater storage capacity is required to build sufficient redundancy into the system. However, this is not explored in this paper.

It is also worth considering that current models do not include decommissioning costs. Some include the assumption that the net cost of decommissioning will be zero due to material and equipment recycling [22], though this remains to be demonstrated in practice. Decommissioning costs are included in this paper's calculation of nuclear hydrogen $LCOH_2$, for both the nuclear plant and the hydrogen generation plant, as decommissioning costs are an up-front consideration for nuclear builds.

In calculating $LCOH_2$ (Equation (2)) the energy source costs have been treated effectively as a utility charge to the hydrogen generation plant. They are captured in terms of the levelised cost of energy (*LCOEnergy*) supplied to the hydrogen generation plant, be it in the form of electricity, heat, or both. *LCOEnergy* must be calculated in the model.

$$LCOH_2 = \frac{LCOEnergy}{efficiency\ of\ HGP} + TOTEX_{HGP} \quad (2)$$

The *LCOEnergy* needs to be divided by the efficiency of the *HGP* (efficiency of HGP, Equation (3)) because it will take more than 1 MJ of input energy to produce 1 MJ of hydrogen, and the levelised cost of energy is the cost per unit of energy input.

$$efficiency\ of\ HGP = \frac{units\ hydrogen\ produced}{units\ energy\ supplied} \quad (3)$$

TOTEX refers to CAPEX + OPEX for the *HGP*, not including the energy costs. The CAPEX and OPEX costs for the hydrogen generation plant are taken from existing literature [23–26]. A discount rate of 5% is applied: a fairly common assumption for medium-risk capital builds.

The levelised cost of energy captures all the costs of the nuclear power plant and expresses it as a cost per unit of heat sent from the nuclear power plant (*NPP*), to the *HGP*. Two key assumptions are made here:

- 100% efficiency of heat transport between *NPP* and *HGP*. In practice, energy losses will occur during transfer and will likely be a function of the distance between the nuclear power plant and the hydrogen generation plant. This is not explored in this work as it is assumed the plants are co-located such that heat energy loss is minimal.
- The model does not consider discrete numbers of nuclear power plants built. The model treats the cost of heat from the reactor as a sort of 'utilities charge', paid per unit of heat by the hydrogen generation plant. In reality, a whole reactor has to be paid for, even if only a fraction of the output is being used. In this work, scenarios are selected so that a discrete number of *HGPs* and *NPPs* are involved to avoid this issue.

The *LCOEnergy* includes both heat and electricity. Fortunately, the efficiency of converting one unit of heat energy into electrical energy is well understood, so all energy can be calculated in terms of the levelised cost of heat (*LCOheat*) according to Equation (4):

$$LCOheat = \frac{cost\ of\ NPP}{units\ of\ heat\ produced} \tag{4}$$

LCOheat is the cost that a unit of heat would need to be charged out at for the *NPP* to break even—this can be effectively treated as a utility charge to the *HGP*. Some of this heat may be used to produce electricity, some may be sent directly to the hydrogen generation plant. The levelised cost of electricity (*LCOE*) can be converted into the levelised cost of heat by multiplying by the efficiency of the *NPP* according to Equation (5):

$$LCOheat = LCOE \times efficiency\ of\ NPP \tag{5}$$

Cost saving can be made on successive builds if learning can be applied, expressed according to Equation (6):

$$C_N = C_0 N^{log_2(1-r\%)} \tag{6}$$

where C_N is the cost of the Nth component, C_0 is the cost of the first component, and r is the learning rate (r = 0.1176 ± 0.0002). The cost reduction observed for successive South Korean nuclear builds [26] has been used to fit these parameters. The same learning rate has been applied to *HGP* cost due to a lack of specific data. While it should be noted that not many other countries have achieved cost reductions from Nth of kind builds, the South Korean data shows what could be possible if the frequency of builds is sufficient to allow this cost reduction (approximately 22 builds in 30 years in the South Korean case).

UK government data predicts the rate at which hydrogen generation technologies are expected to mature. Specifically, it predicts improvements in efficiency up to the year 2050 [27]. A polynomial was fitted to this data for *HTSE*, however, the government report did not include any data on thermochemical processes, due to the low TRL of these technologies this would be impossible to determine at this stage in development.

Thermochemical hydrogen production process models have been developed for the sulphur iodine (*SI*) cycle, the Hybrid Sulphur (HyS) a.k.a. Westinghouse cycle, and the Copper Chlorine (CuCl) cycle. Of these three, *SI* was estimated to have the greatest potential efficiency, although the most efficient range of this estimate would require significant heat integration and work on catalysis to improve yields. Therefore, *SI* was selected as the best comparator to *HTSE* for this study.

The efficiency improvement correlation in Equation (7) was developed for *HTSE*, assuming that 85% of the total input energy is supplied as electricity, with the remaining 15% as heat [8]:

$$HTSE\ Efficiency = \frac{0.85}{\left(\frac{7.18076 \times 10^{15}}{year^4} - \frac{7.01654 \times 10^{12}}{year^3} + \frac{1.71775 \times 10^{9}}{year^2}\right)} \tag{7}$$

In order to create the efficiency improvement correlation for *SI* in Equation (8), an 'offset', x (i.e., how many years behind *SI* is relative to *HTSE*) is added to the expression:

$$SI\ Efficiency = \frac{maximum\ theoretical\ efficiency \times 0.85}{\left(\frac{7.18076 \times 15}{(year - x)^4} - \frac{7.01654\ \times 12}{(year - x)^3} + \frac{1.71775 \times 9}{(year - x)^2}\right)} \tag{8}$$

As a function of the commissioning year, the efficiencies tend towards the maximum that is assumed possible at full maturation based on current understanding. This is not 100% for thermochemical technologies due to heat loss. However, developments in heat integration could raise the efficiency from 40% to 80% [10]. The top end of this potential efficiency range is quite optimistic, therefore, in this analysis, a mid-point of 60% is also considered, and an offset of 0, 15, and 30 years is explored. Ideally, efficiency would be expressed in terms of the plant temperature, but there is insufficient data to underpin this.

2.3. Scenarios of Interest

The techno-economic assessment was performed for two coupling scenarios:

- *HTSE* coupled to a High Temperature Gas Reactor (HTGR) at 1093 MW thermal and a nuclear gas turbine efficiency of 40%, with 85% of the power input to the electrolyser in the form of electricity, and the remaining 15% as heat;

- An *SI* cycle coupled to a HTGR reactor at 1261.4 MWth.

Baseline CAPEX and OPEX data are taken from the literature ([8] and [23] respectively), and the model then predicts how $LCOH_2$ might vary as a function of the commissioning year and the build number (N^{th} of a kind). It is expected that a demonstration HTGR will be operational in the UK in the early 2030s [28].

2.4. HTSE Process Model

2.4.1. Electrolysis of Water

Through electrolysis, liquid water or steam can be separated into hydrogen and oxygen (Equation (9)):

$$H_2O \leftrightarrow H_2 + \frac{1}{2}O_2 \tag{9}$$

This reaction is a non-spontaneous endothermic reaction, requiring inputs of work and heat (Equation (10)); with at least the work component being supplied wholly by electrical energy:

$$\Delta H_R = \Delta G_R + (T\,\Delta S_R) \tag{10}$$

where the specific total energy demand of the reaction (equivalent to the enthalpy change ΔH_R) is the sum of the work requirement (the Gibbs free energy change ΔG_R) and the heat requirement (the absolute temperature T multiplied by the entropy change ΔS_R).

Theoretically, the minimum potential difference required to drive an electrochemical reaction and supply the work requirement in an electrochemical cell can be related to Gibbs free energy change of the reaction, this voltage is known as the thermodynamic voltage V_{td} (Equation (11)):

$$V_{td} = \frac{\Delta G_R}{z\,F} \tag{11}$$

where F is Faraday's constant (96,485 C mol^{-1}), and z is the number of electrons transferred in the reaction (in the case of water electrolysis: 2 per mol H_2).

The voltage that would be required to theoretically provide the total energy needed by the reaction, providing the work component as well as extra electrical energy to cover the heat requirement (through losses that end up as thermal energy in a cell), is known as the thermoneutral voltage; meaning an electrolysis cell that was perfectly insulated would remain at a constant temperature when operated with this voltage. The thermoneutral voltage V_{tn} can be related to the enthalpy change of the reaction according to Equation (12):

$$V_{tn} = \frac{\Delta H_R}{z\,F} \tag{12}$$

Applying a potential difference V_{cell} over an electrochemical cell, large enough to overcome activation energies, results in the desired reaction occurring. This cell load will then be, as in Equation (13), the sum of V_{td} as well as practical losses, known as overpotentials:

$$V_{cell} = V_{td} + (V_{conc} + V_{act,c} + V_{act,a} + V_{ohmic}) \tag{13}$$

where:

- V_{conc} is associated with losses incurred in driving material flows of the reactants towards reaction sites in the cathode or anode;
- $V_{act,c}$ and $V_{act,a}$ are associated with losses related to overcoming the activation potential of the reactions and electron transfer with the electrode in the cathode and anode respectively, they are related to electrode material properties and reduced by effective electrocatalysts;
- V_{ohmic} is associated with losses due to electrical resistance in the cell components, for example, the resistance of the electrolyte, or electrode materials.

The difference between the operating voltage of an electrochemical cell and the thermoneutral voltage, multiplied by the current through the cell, can be used to calculate the net excess heat (Equation (14)) i.e., the heat produced by the cell (if $V_{cell} > V_{tn}$), or the net heat deficit i.e., the heat taken in by the cell (if $V_{cell} < V_{tn}$):

$$Q_{cell} = I\,(V_{cell} - V_{tn}) \tag{14}$$

where I is the current through the electrochemical cell.

When splitting liquid water in alkaline or PEM (proton exchange membrane, also known as polymer electrolyte membrane) electrolysers, overpotentials are relatively high, requiring a high V_{cell} (significantly above V_{tn}) and generating more than enough heat to cover the heat requirement of the reaction along with waste heat; practical liquid water electrolyser systems generally require active cooling. Higher temperature steam electrolysis systems instead can operate at or below V_{tn} and thereby increase electrical efficiency.

The molar rate of hydrogen produced $m_{H_2\,gen}$ by an electrochemical cell is proportional to the electrical current through it as in Equation (15):

$$m_{H_2\,gen} = \delta \frac{I}{z\,F} = \frac{1}{2} m_{O_2\,gen} = m_{H_2O\,con} \tag{15}$$

where:

- δ is the Faraday efficiency, the selectivity of current directed to the desired reaction versus undesired side reactions
- $m_{O_2\,gen}$ is the molar rate of oxygen generation.
- $m_{H_2O\,con}$ is the molar rate of water consumption.

2.4.2. Solid Oxide Electrolysis Cell Model

Solid oxide electrolysis cells (SOECs), also known as solid oxide steam electrolysis (SOSE) cells can process high temperature steam, rather than liquid water, to conduct *HTSE*. An advantage to carrying out electrolysis at higher temperatures is that, as the temperature climbs, the Gibbs free energy change of the water dissociation reaction decreases, and hence the work requirement for the reaction also decreases, at the expense of a greater heat requirement. See Figure 1.

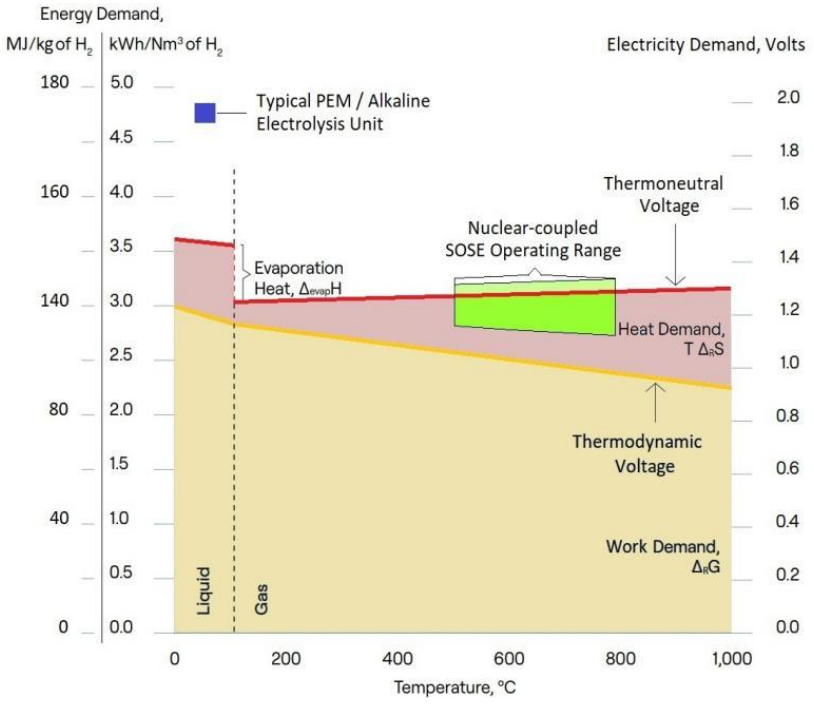

Figure 1. Energy Demand for Electrolysis.

As the Gibbs free energy change of reaction is lower, the thermodynamic voltage decreases, and also at those higher temperatures, SOEC materials typically exhibit lower electrical resistances and improved reaction kinetics, this allows a high current density and hence high hydrogen production rate to be achieved at much lower cell voltages than for liquid water electrolysis. The practical operating voltage can even be lower than the red (thermoneutral) line in Figure 1, making use of extra external heat input to the system to maintain the electrolyser's temperature while achieving even greater electrical efficiencies.

Since the conversion of heat to electrical energy in modern nuclear power stations using a Rankine cycle is typically 33–42% efficient, then using heat from the reactor loops directly is advantageous because doing so bypasses this inefficiency. This requires a closer coupling to the reactor than for liquid electrolysis because steam must be taken from and returned to somewhere in the secondary loop, however there are numerous options for locations to withdraw steam in a typical turbine layout.

For SOECs the electrolytic cell consists of a solid oxide electrolyte with porous conducting electrodes deposited on either side, see Figure 2.

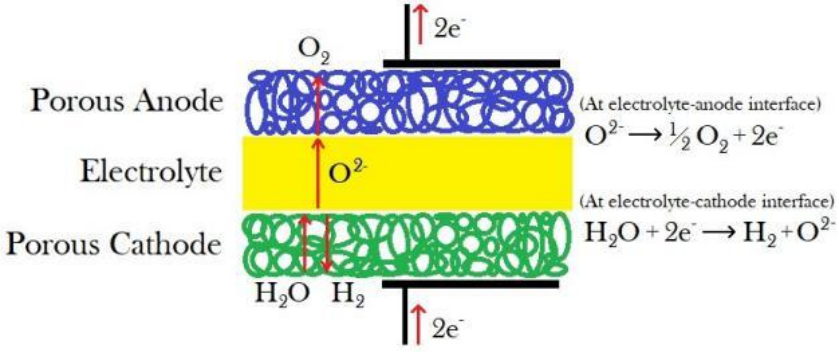

Figure 2. H_2 Production in an SOEC.

The electrolyte is an oxygen-conducting ceramic oxide, a typical material is yttria-stabilized zirconia (Y_2O_3-ZrO_2) also known as YSZ. Variations on this material are used in different concepts and industrial designs. The important feature of this material is that it contains channels along which (only) oxygen anions can diffuse. The cathode in this model is taken to be nickel-YSZ while the anode in this model is taken to be strontium doped lanthanum manganoxide (LSM).

In this design, steam is supplied to the porous cathode and, when sufficient electrical potential is applied between the two electrodes; the water molecules dissociate to form hydrogen gas and oxygen ions at the cathode -electrolyte interface (Equation (16)).

$$H_2O + 2e^- \leftrightarrow H_2 + O^{2-} \tag{16}$$

The oxygen ions are transported through the electrolyte to the anode due to the potential difference and oxidised at the electrolyte-anode interface (Equation (17)).

$$O^{2-} \leftrightarrow \frac{1}{2}O_2 + 2e^- \tag{17}$$

Air is used as a sweep gas, inlet to the anode side to remove oxygen, dilute the oxygen concentration, and thus both increase the diffusion rate of oxygen ions and decrease the rate of corrosion.

On the cathode side, a portion of the outlet is returned as a recycle and mixed in with the inlet, to ensure the inlet contains a fraction of hydrogen; the purpose of this is to maintain reducing conditions, scavenge oxygen through the back reaction and avoid oxidation of the nickel in the cathode on the portions of the cell close to the inlet—thus increasing cell performance and longevity.

The planar stack design modelled is as in Figure 3, with the H_2O + H_2 cathode side streams and the O_2 + air anode side streams flowing perpendicular to one another. This required the model of each cell to be discretised in two dimensions, represented by 400 nodes per cell connected in parallel, considering local partial pressures, current density, and temperature. Material and energy balances are carried out over each node, with the cathode side flowing between nodes in one direction and the anode side flowing between nodes in the perpendicular direction. Each cell in the stack is connected to the others in series; the cathode side and anode side inlets to the stack are divided equally by the number of cells before being distributed to each cell in the series, and the outlets of each cell are collected and mixed in a cathode side exhaust and an anode side exhaust.

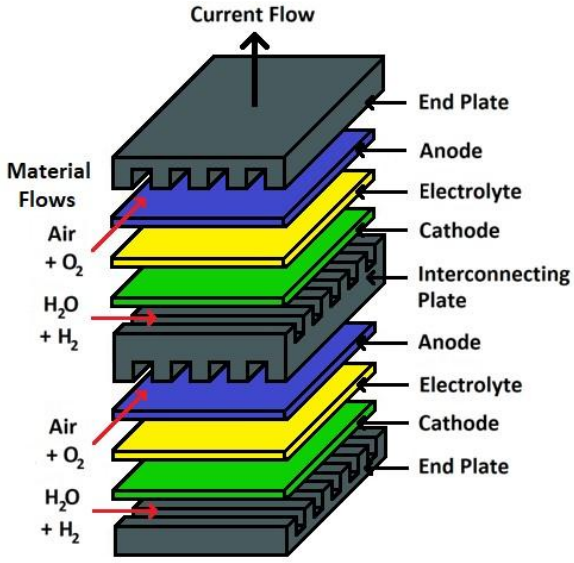

Figure 3. Exploded-view SOEC Stack, perpendicular planar arrangement.

To prevent significant concentration and ohmic overpotentials, the cells are made as thin as is practicable, there are also commercial designs of SOECs that follow a tubular arrangement.

The cell voltage V_{cell} is determined with Equation (13), the terms of which shall now be discussed.

The standard thermodynamic potential V_{td}^0 is temperature dependant; varying more significantly over the possible operating temperature range of an SOEC than over the relatively small operating temperature range of alkaline and PEM electrolysers; substituting Equation (10) into Equation (11) results in Equation (18):

$$V_{td}^0 = T\left(\frac{\Delta S_R^0}{nF}\right) + \frac{\Delta H_R^0}{nF} \tag{18}$$

ΔS_R^0 and ΔH_R^0 are themselves temperature dependant but may be calculated at any temperature through correlations from thermodynamic tables. For the reaction of the dissociation of steam, this can be approximated by Equation (19):

$$V_{td}^0 = 1.29 - 0.000292(T - 273.15) \tag{19}$$

for temperature in K over the temperature range between T = 773 − 1773 K [29].

Then, the thermodynamic voltage under cell operating conditions can be found using the Nernst equation (Equation (20)):

$$V_{td} = V_{td}^0 + \frac{RT}{zF}\, ln\left(\frac{P_{H_2}\, P_{O_2}^{0.5}}{P_{H_2O}}\right) \tag{20}$$

where the partial pressures P_{H_2}, P_{O_2} and P_{H_2O} of the respective species are assumed to be those of the bulk stream at that point in the cell, represented by a discretised node.

The cathode and anode activation overpotentials $V_{act\,c/a}$ can be expressed by the Butler-Volmer equation (Equation (21)), assuming a symmetric electron transfer which is common in literature.

$$V_{act\,c/a} = \frac{2\,RT}{zF} sinh^{-1}\frac{J}{2J_{0\,c/a}} \tag{21}$$

where $J_{0\,c/a}$ represents the exchange current densities of the cathode and anode.

The concentration overpotential in the cathode is found by Equation (22), derived in [30]:

$$V_{conc} = -\frac{RT}{2F} ln\left(\frac{\left(1-\frac{JRTd_c}{2FD_{eff\,H_2O}P_{H_2O}}\right)}{1+\frac{JRTd_c}{2FD_{eff\,H_2O}P_{H_2}}}\right) \tag{22}$$

where:

- $D_{eff\,H_2O}$ = the effective diffusion coefficient of steam in the cathode, which is a combination of Knudsen and molecular binary diffusion;
- d_c is the depth of the cathode layer.

The effective diffusion coefficient can be expressed using Equation (23) by combining the diffusion mechanisms of molecular diffusion (governed by molecule-molecule interactions, and Knudsen diffusion, governed by molecule-pore interaction:

$$\frac{1}{D_{H_2O}^{eff}} = \frac{\omega_c}{\emptyset_c}\frac{1}{D_{H_2-H_2O}} + \frac{1}{D_{H_2O,k}} \tag{23}$$

where $\omega_c/\emptyset_c$ is the ratio of the cathode tortuosity to porosity, $1/D_{H_2-H_2O}$ is the reciprocal of the molecular diffusion coefficient, and $1/D_{H_2O,k}$ is the reciprocal of the Knudsen diffusion coefficient.

$D_{H_2O,k}$ can be modelled using kinetic theory (Equation (24)):

$$D_{H_2O,k} = \frac{2}{3}r_{cp}\sqrt{\frac{8RT}{\pi M_{H_2O}}} \tag{24}$$

where r_{cp} is the radius of a pore in the cathode, and M_{H_2O} is the molecular mass of H_2O.

$D_{H_2-H_2O}$ can be found via the Chapman-Enskog theory of ideal gases (Equation (25)):

$$D_{H_2-H_2O} = 0.00133\left(\frac{1}{M_{H_2}}+\frac{1}{M_{H_2O}}\right)^{1/2}\frac{T^{3/2}}{P\sigma_{H_2O,H_2}\Omega_D} \tag{25}$$

where P is the bulk total pressure in the cathode of the node, M_{H_2} is the molecular mass of hydrogen, σ_{H_2O,H_2} is the mean characteristic length of the diffusing species (Equation (26)):

$$\sigma_{H_2O,H_2} = \frac{\sigma_{H_2O}+\sigma_{H_2}}{2} \tag{26}$$

And the dimensionless collision coefficient Ω_D is found by Equation (27):

$$\Omega_D = \frac{1.06}{\tau^{0.156}} + \frac{0.193}{exp\,(0.476\tau)} + \frac{1.036}{exp\,(1.53\tau)} + \frac{1.765}{3.894\tau} \tag{27}$$

where the dimensionless temperature τ is found by Equation (28):

$$\tau = \frac{kT}{\varepsilon_{H_2O,H_2}} \tag{28}$$

Values for $\sigma_{H_2O}$and σ_{H_2} are given in [30] as 2.641Å and 2.827Å, respectively, while values of ε/k for H_2O, H_2 are given as 809.1 K and 59.7 K.

The anode concentration overpotential is set equal to zero because the O^{2-} ions are fully oxidised at the electrolyte-anode interface without any diffusion in the porous anode significantly limiting the reaction.

In SOECs the electrodes generally have much higher electrical conductivity than the electrolyte, the electrolyte and its resistance to the O^{2-} transfer is the limiting factor, and so the ohmic overpotential is assumed to be proportional to electrolyte resistance (Equation (29)):

$$V_{ohmic} = Jd_eR_e \tag{29}$$

where d_e is the depth of the electrolyte layer. The resistance of the electrolyte is temperature dependant; and for this electrolyte, the following expression (Equation (30)) from [31] is used:

$$R_e(\Omega m) = 2.99 \times 10^{-5} e^{\left(\frac{10300}{T}\right)} \tag{30}$$

where T is the absolute temperature in K.

Parameters used in the SOSE model are collated in Table 1:

Table 1. SOEC parameters.

Parameter	Value	Units	Reference
Depth of electrolyte layer, d_e	8	μm	[32]
Depth of cathode layer, d_c	8	μm	[32]
Radius of pore in cathode, r_{cp}	0.5	μm	[30]
Cathode porosity, $\emptyset_c$	0.4	-	[32]
Cathode tortuosity, ω_c	6	-	[30]
Exchange current densities:			
Cathode, $J_{0\,c}$	5500	A m^{-2}	[30]
Anode, $J_{0\,a}$	2100	A m^{-2}	[30]

The electrolysis stack is placed within a flowsheet as depicted in Figure 4, in which the inlets to the stack (steam on the cathode side, sweep air on the anode side) are brought up to the stack operating temperature by a combination of heat transfer and integration with the stack exhaust streams, electrical heaters as well as heat transfer from low temperature (LT) steam and (optionally) high temperature (HT) steam derived from a nuclear reactor.

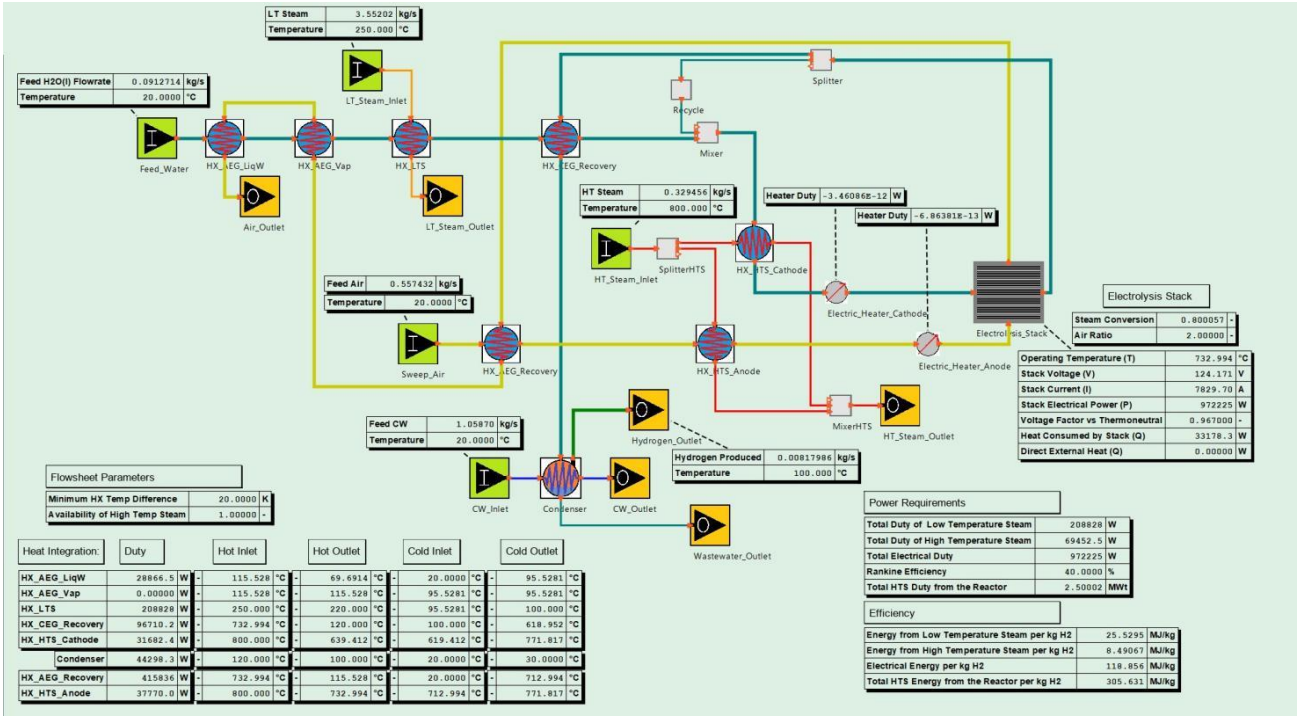

Figure 4. *HTSE* flowsheet model.

Most of the external energy input is only needed at relatively low temperatures >100 °C to vaporise the feed steam. When high temperature (>600 °C) steam is available this improves system efficiencies slightly.

The product cathode exhaust gas is eventually put through a condenser using cooling water to remove residual H_2O, the H_2 product could then be fully dried by desiccant scrubbing.

It was found that if low temperature heat from a nuclear reactor was available, but not high temperature heat (for example from a HTGR), then running the stack slightly above (V_{cell} = 1.02 V_{tn}) thermoneutral results in the highest system efficiencies. If high temperature heat is available, then running the stack slightly below (V_{cell} = 0.94 V_{tn}) thermoneutral results in the highest system efficiencies.

The following test model conditions specified in Table 2 produced 327 Nm^3/h of H_2 at steady state, with a system efficiency of 305 MJ of heat from reactors per kg of H_2 produced. A range of results were scaled to match the scenario used in the economic analysis.

Table 2. *HTSE* Flowsheet steady state process parameters.

Parameter	Value	Units
Active area of a cell	0.1	m^2
Number of cells	1000	-
Stack operating temperature	733	°C
Stack voltage	1240	V
Stack current	783	A
Reactor heat allocated to H_2 production	-	-
Via Electricity	972	kW
As LT Steam	209	kW
As HT Steam	69	kW
Steam Conversion (Fraction of steam inlet to stack consumed)	0.8	-
Air ratio (O_2 inlet / produced)	2	-
Fraction of cathode side exhaust recycled to inlet	0.5	-
Minimum temperature difference for heat exchange	20	°C

2.5. SI Cycle Process Model

The goal of a hydrogen-producing thermochemical cycle is to find a sequence of chemical reactions that, overall, consume water and produce hydrogen (with oxygen as a by-product) while requiring minimum heat input, producing no additional products and consuming no additional reagents, resulting in an autocatalytic cycle.

The *SI* cycle is one such thermochemical cycle made up of three reactions:

(1) Bunsen Reaction (~120 °C, liquid phase), Equation (31):

$$SO_2(g) + I_2(l) + 2H_2O(l) \rightarrow H_2SO_4(aq) + 2HI(aq) \quad (31)$$

This reaction is exothermic and so requires cooling to achieve the desired efficiency. The product of the reaction is a two-phase solution, with a light phase containing sulphuric acid and a heavy phase containing iodine and hydrogen iodide. The phases are separated and then are directed towards the two follow up reactors.

(2) H_2SO_4 Decomposition (700–800 °C, gas phase), Equation (32):

$$H_2SO_4(g) \rightarrow H_2O(g) + SO_2(g) + \frac{1}{2}O_2(g) \quad (32)$$

The light phase from the Bunsen reaction is distilled to form a sulphuric acid stream which then undergoes sulphuric acid decomposition in the gas phase. This reaction is endothermic, requiring a heat input to sustain. The H_2O and SO_2 products, along with the water from the distillation of sulphuric acid, are recycled back to the Bunsen reaction whereas the O_2 is removed as an overall cycle product.

(3) *HI* Decomposition (400–550 °C, gas phase), Equation (33):

$$HI(g) \rightarrow \frac{1}{2}H_2(g) + \frac{1}{2}I_2(g) \tag{33}$$

The heavier phase from the Bunsen reaction is boiled to form a vapour which undergoes hydrogen iodide decomposition. This reaction is endothermic, requiring a heat input to sustain. The I_2 product is recycled back to the Bunsen reaction whereas the H_2 is removed as the overall cycle product.

Fresh H_2O must be supplied to the Bunsen reaction to sustain the cycle. The overall reaction of the cycle is then the same as Equation (9).

In the model of this process, each of the reactions takes place within its own reaction chamber, and the flowsheet and separation pathways follow the design depicted in Figure 5.

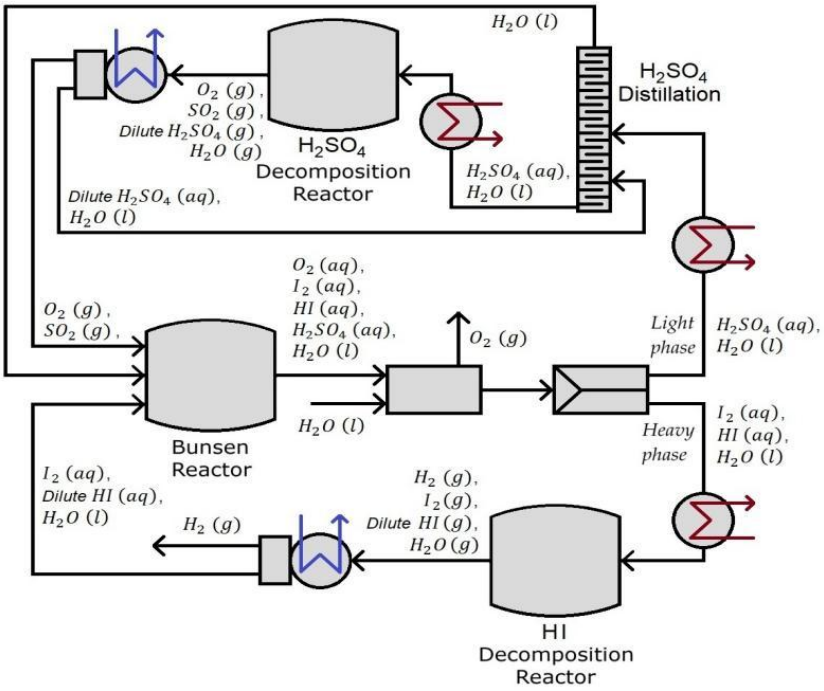

Figure 5. *SI* Cycle Flowsheet.

Model basis and assumptions:

- Inlets of I_2 and SO_2 to the Bunsen reactor are closed once steady state operating conditions are reached;
- Simplified reaction kinetics, assuming that each reaction is elementary; assuming that the first step (breakdown to SO_3 + H_2O) in the two-step decomposition of H_2SO_4 is instantaneous above 700 °C and so this reaction is limited by the subsequent reduction of SO_3 to SO_2;
- The temperature and pressure in each reaction chamber, the water inlet flowrate to the system, and the flowrate out of each reaction chamber are all controlled by manually tuned PI (Proportional-Integral) controllers;
- A detailed heat integration analysis was not performed however the power required to change the temperature of streams and to maintain reaction chamber temperatures is calculated;
- Mixing and separation units were assumed to be 100% efficient, but the equipment to achieve this was not sized;
- Power to operate the wider flowsheet around the electrolyser is not considered (e.g., energy requirements for pumping were neglected);

- All three reactors are assumed to be well mixed systems and the mixture properties are calculated for an ideal mixture.

The governing equations which characterise the liquid phase and gas phase reaction chambers, as well as kinetic parameters, are given in Appendix A. It is noted that some of these assumptions are known to be gross approximations, a specific example being the phase equilibrium in these process steps. For this reason, this process can be judged to be relatively immature and this should be taken into account when reviewing the economic data. Setting aside these concerns, $LCOH_2$ can however be used to assess the potential of this technology and drive the need for R&D to underpin the assumptions which have been outlined.

The following test model conditions specified in Table 3 produced 320 Nm^3/h of H_2 at a steady state, these results were scaled to match the scenario used in the economic analysis.

Table 3. *SI* cycle steady state process parameters.

Parameter	Value	Units
Bunsen Reactor		
Setpoint Temperature	120	°C
Liquid Volume Setpoint	4.5	m^2
H_2SO_4 Decomposition Reactor		
Setpoint Temperature	720	°C
Volume	1	m^2
Pressure Setpoint	7	bar
HI Decomposition Reactor		
Setpoint Temperature	450	°C
Volume	10	m^2
Pressure Setpoint	22	bar
H_2O inlet flowrate	4	mol/s

2.6. Integration and Counterfactuals

The thermochemical process models were used to calculate the possible efficiencies of a hydrogen generation plant, as a function of the heat exchange within the process. This efficiency was then used by the technoeconomic model when calculating possible $LCOH_2$. Where there was a range of possible process efficiencies, an upper and lower bound were used, as well as a mid-point, to make $LCOH_2$ estimates.

The $LCOH_2$ of nuclear-hydrogen couplings must be compared to other production routes in order to determine cost-competitiveness. Offshore wind scenarios are selected to represent renewables and 'green' hydrogen in the UK [33], and Steam Methane Reformation (SMR) [22] and Autothermal Reformation (ATR) [34] with carbon capture and storage are selected to represent 'blue' hydrogen. Published estimates of $LCOH_2$ from other authors are used to make this comparison: the UK Offshore Renewable Energy Catapult, the IEA Greenhouse Gas R&D Programme, and Phase 1 of the BEIS hydrogen supply Programme: HyNet Low Carbon Hydrogen Plant respectively.

3. Results of Economic Analysis

Table 4 gives the levelised cost of electricity and heat for the *NPP* which are key inputs to the economic model:

Table 4. *LCOE* and *LCOheat* for Nth of a kind HTGRs.

Nth of a Kind HTGR	*LCOE* (£/MWh)	*LCOheat* (£/MWh)
1	29.4–33.0	14.7–15.5
10	23.7–24.8	11.9–12.4

Table 5 shows that the *SI* process is predicted to have the best process efficiency of the thermochemical processes studied. This is why *SI* was chosen as the best comparator for *HTSE* in the technoeconomic assessment. All costs in the results section are normalised to 2016 values, including the counterfactuals. Process model descriptions for the CuCl and HyS cycles are available as supplementary material.

Table 5. Efficiencies calculated by the process models for hydrogen production processes.

Technology	MJ of Reactor Heat Required to Produce 1 kg H_2	Efficiency (High Heating Value H_2 = 141.9 MJ/kg)
PEM	470	30.2%
HTSE	330–300	43–47.3%
SI	297–174	47.8–81.6%
HyS	546–293	26.0–48.4%

In line with the range of efficiency predicted by the technical modelling work, three values for the efficiency of the *SI* cycle to tend towards are selected: 80%, 40%, and a mid-point of 60%. The results for each of these efficiency estimates are shown in Table 6 for 1st of a kind builds, and Table 7 for 10th of a kind builds.

Table 6. $LCOH_2$ predictions in £/kg for 1st of a kind plants.

Technology	Commissioning Year: 2040	Commissioning Year: 2050
HTSE	2.16	2.14
SI with 80% efficiency	1.32–1.57	1.31–1.45
SI with 60% efficiency	1.77–2.09	1.89–1.94
SI with 40% efficiency	2.62–3.10	2.59–2.88

Table 7. $LCOH_2$ predictions in £/kg for 10th of a kind plants.

Technology	Commissioning Year: 2040	Commissioning Year: 2050
HTSE	1.55	1.53
SI with 80% efficiency	1.04–1.23	1.03–1.14
SI with 60% efficiency	1.39–1.64	1.37–1.52
SI with 40% efficiency	2.06–2.44	2.03–2.26

Commissioning year has a small impact on $LCOH_2$ for *HTSE*, and a slightly larger impact on *SI* of all efficiencies, with little difference between 1st and 10th of a kind builds. This is because the maturation rate is a function of the year, not the number of builds, in the model calculations, and a more sophisticated estimate might

take both into account. With all other parameters equal, the difference between 1st and 10th of a kind builds is significant, reducing costs by around 20–30%. However, as previously noted, this assumes a build rate of almost one plant per year.

To compare these estimates with those for non-nuclear sources, they are plotted against counterfactuals from offshore wind [33], Steam Methane Reformation, [22] and Autothermal Reformation (ATR) [34] in Figure 6.

Based on the current set of assumptions, Tables 6 and 7 suggest that in order for the *SI* process to compete with *HTSE*, it would have to have a minimum efficiency of greater than 60%. The greatest impact by far is made by the assumed future practical efficiency of the *SI* process: between 40–80% the $LCOH_2$ approximately halves and a 40% efficiency would not be sufficient to be competitive. This highlights the importance of heat integration to the $LCOH_2$ for the *SI* process. Figure 6A shows that, under the current assumptions, a nuclear-*SI* coupling with a possible *SI* efficiency of 40% is unlikely to compete economically with alternatives. With an *SI* efficiency of 80%, this coupling would outperform almost all technologies economically, with only autothermal reformation with carbon capture possibly proving cheaper before 2040. A greater understanding of the limitations (and costs) of heat integration in the *SI* cycle is essential to narrowing this uncertainty range. Furthermore, given the assumptions with respect to phase equilibria, it is highly unlikely that experimental *SI* plants operating today achieve an overall efficiency of 10%, substantially below the minimum required for this technology to be competitive with *HTSE*. Substantial improvements in suitable heterogeneous catalysts would be required to close this efficiency gap [35,36].

If an *SI* cycle efficiency of 60% can be achieved, as in Figure 6B, the effects of the 'offset' years can be seen. This refers to how many years behind the development of *HTSE SI* is believed to be, i.e., if *HTSE* has a TRL of 7 now (as an industrial scale demonstrator is being established), then the 'offset' predicts how many more years it will be until *SI* is also mature enough (currently TRL < 3) for an industrial-scale demonstrator to be sensible. To some extent, this offset can be adjusted by increases and decreases in funding and research. The technology development could be accelerated beyond the algorithm's current predictions, with concentrated effort. The effect of the offset is also significant (though less so than efficiency). This could make the difference between competing with only 1st of a kind *HTSE* in 2040, and outperforming all except autothermal reformation and 50th of a kind *HTSE*.

Of course, reductions in plant CAPEX can make a big difference to $LCOH_2$. $LCOH_2$ is predicted to drop by around 28% between the 1st and 10th build of a *HTSE*, if the learning rate is applied to CAPEX costs. The effect of the discount rate has not been explored here, but previous work has shown its impact on $LCOH_2$ to be sizeable [37].

4. Discussion

HTSE offers significantly greater efficiencies than liquid water electrolysis through the use of nuclear heat, and this $LCOH_2$ analysis has shown that nuclear coupled *HTSE* should be competitive with hydrogen generated from renewables on a purely cost basis; this is without even accounting for the inherent advantages of a nuclear coupled technology such as: high scale, high capacity factor, flexibility in siting close to users, and non-intermittent supply reducing buffer storage requirements. *HTSE* remains the most promising hydrogen generating technology to couple with nuclear energy for at least the medium-term future, as thermochemical methods are unlikely to reach the market in a form where they could economically compete in this time period.

By the 2040s and beyond, when the UK's Advanced Modular Reactor (AMR) programme, with its interest in HTGRs, coincides with the potential arrival of operational-scale thermochemical hydrogen production technologies, thermochemical technologies could begin to compete with *HTSE* technology. This analysis shows that to maximise the benefits of nuclear power for hydrogen production, both high temperature reactors and thermochemical technologies that exploit them should be developed in parallel. Whilst this could present an opportunity for national governments wishing to decarbonise most cost-effectively, additional understanding is required to accurately assess the scope of this opportunity.

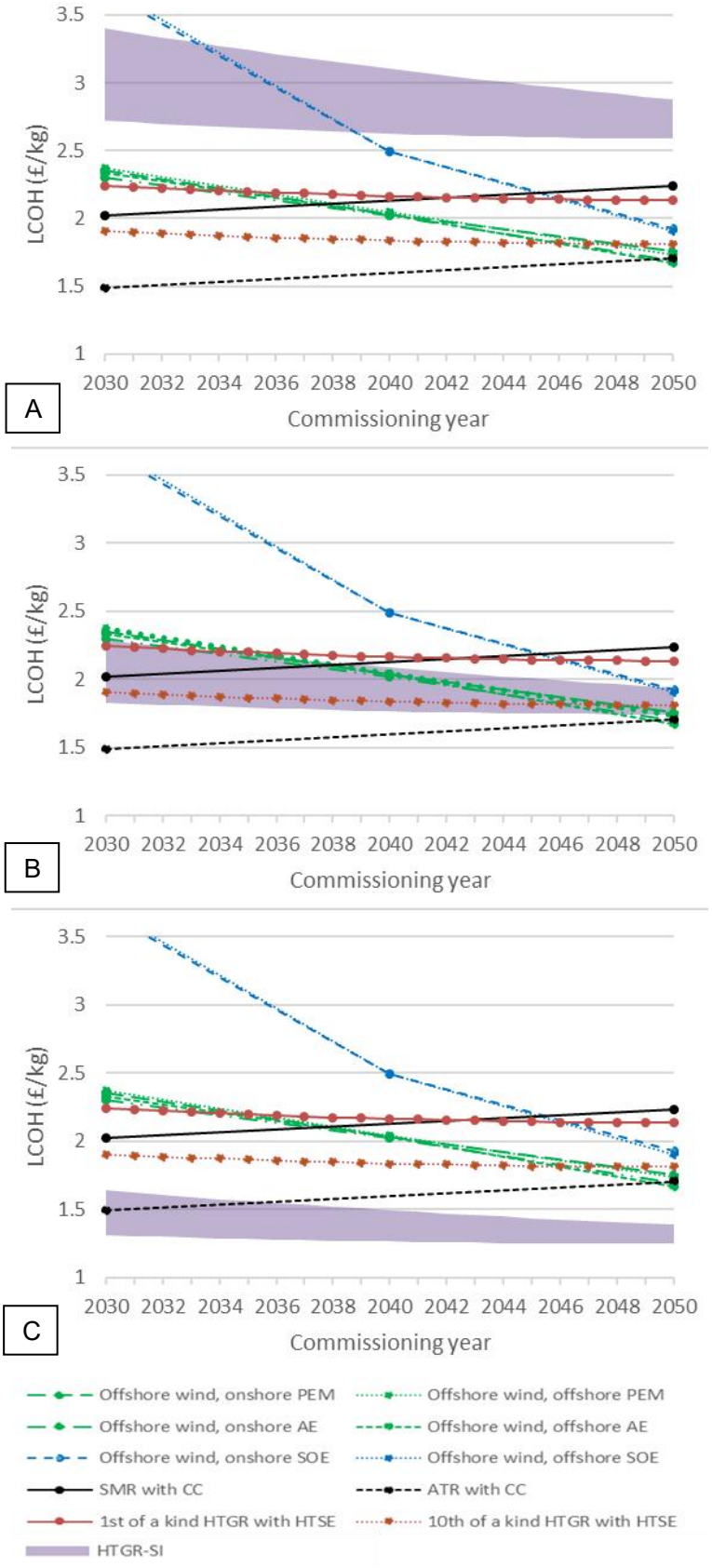

Figure 6. Comparison of nuclear and non-nuclear hydrogen generation costs, assuming an efficiency for *SI* plants of 40% (**A**), 60% (**B**) and 80% (**C**).

It is important to remember that $LCOH_2$ is just one measure of the economic performance of a system. $LCOH_2$ does not capture the ability of a system to match supply to demand, and takes account only of cost, not of pricing structures. More significantly perhaps it neglects the impact on the economy as a whole (gross value add) which could be a major differentiator when considering the coupling between energy security and climate change.

5. Conclusions

This paper identifies a series of conditions that, if met, would make nuclear-*HTSE* and nuclear-thermochemical couplings a highly attractive option:

- Reduce CAPEX by realising cost savings due to learning in successive HTGR-*HTSE* builds;
- Development of catalysis and heat integration systems to achieve a theoretical hydrogen production efficiency of around 60 % for the *SI* cycle;
- Accelerate the maturation rate of thermochemical technology through research and development to close the TRL gap (from current TRL < 3).

Currently, the efficiencies reported by process models of individual hydrogen production technologies are used by the techno-economic model, but there is an ambition to more closely integrate these modules in future.

Author Contributions

The authors confirm their contribution to the paper as follows: manuscript authoring, process modelling of *HTSE* and *SI* Cycle: C.C.; process model checking: R.J.; manuscript preparation and techno-economic modelling: K.T.; techno-economic model checking: J.D.; technical vision and manuscript authoring: M.B.

Funding

This work was partly supported by the UK Government Department for Business Energy and Industrial Strategy (BEIS).

Institutional Review Board Statement

Not applicable.

Informed Consent Statement

Not applicable.

Acknowledgments

We would like to acknowledge Allan Simpson, Chief Technologist at Equilibrion, for setting out the strategic vision for hydrogen during his time in NNL and acting as the technical lead on the HyTN project, which contributed to this work.

Conflicts of Interest

The authors declare no conflict of interest.

Appendix A

The governing equations of the *SI* Cycle gas phase reaction chambers are as follows (Equations (A1)–(A16)):

$$\frac{dM_i}{dt} = m_{i,in} - y_i m_{out} + V_R v_i r \tag{A1}$$

$$M_i = y_i M_R \tag{A2}$$

$$\sum_i y_i = 1 \quad or \quad \sum_i M_i = M_R \tag{A3}$$

$$m_{in} = \sum_i m_{i,in} \tag{A4}$$

$$P_R V_R = M_R R T_R \tag{A5}$$

$$m_{out} = MAX(f_P(P_R - P_{outlet}), 0) \tag{A6}$$

$$r = f(T_R, C_i) \tag{A7}$$

$$C_i = \frac{y_i M_R}{V_R} \tag{A8}$$

$$\frac{dU_R}{dt} = -\sum_i m_{i,in} \Delta h_{i,T_{in},T_R} - \Delta h_{RXN} r + q_{HX} \tag{A9}$$

$$U_R = M_R h_R - P_R V_R \tag{A10}$$

$$h_R = \sum_i y_i h_{i,T_R} \tag{A11}$$

$$\Delta h_{i,T_{in},T_R} = h_{i,T_{in}} - h_{i,T_R} \tag{A12}$$

$$\Delta h_{RXN} = f(T_R) \tag{A13}$$

$$h_{i,T_{in}} = f(T_{in}) \tag{A14}$$

$$h_{i,T_R} = f(T_R) \tag{A15}$$

$$q_{HX} = f_T\left(T_R - T_{setpoint}\right) \tag{A16}$$

where:
m_{in} = the total molar flowrate of material into the reaction chamber;
m_{out} = the total molar flowrate of material out of the reaction chamber;
y_i = the mole fraction of component i within the reaction chamber;
M_i = the molar inventory of component i within the reaction chamber;
M_R = the total molar inventory within the reaction chamber;
V_R = the volume of the reaction chamber;
T_R = temperature within the reaction chamber;
P_R = pressure within the reaction chamber;
P_{outlet} = pressure of the reaction chamber outlet (f_P represents a PI function) (specified);
r = the volume specific molar rate of reaction, a function of T_R and C_i (i = 1,2…n);
v_i = the stoichiometric coefficient of component i in the reaction;
C_i = the concentration of component i within the reaction chamber;
U_R = the internal energy of the reactor system;
h_R = the molar specific enthalpy of the reactor system.
h_{i,T_R} = the enthalpy of component i at T_R;
$h_{i,T_{in}}$ = the enthalpy of component i at the inlet temperature, T_{in};
$\Delta h_{i,T_{in},T_R}$ = the molar specific enthalpy change required by the reactor system to change component i from the inlet temperature to the temperature of the reactor contents;
h_{RXN} = the enthalpy of reaction (a function of T_R);
q_{HX} = the heat flux from outside the reactor system;
$T_{setpoint}$ = the setpoint temperature for the reactor (f_T represents a PI function).

The governing equations of the *SI* cycle liquid phase reaction chamber are as follows (Equations (A17)–(A33)):

$$\frac{dM_i}{dt} = m_{i,in} - x_i m_{out} + V_L v_i r \tag{A17}$$

$$M_i = x_i M_R \tag{A18}$$

$$\sum_i x_i = 1 \quad or \quad \sum_i M_i = M_R \tag{A19}$$

$$m_{in} = \sum_i m_{i,in} \tag{A20}$$

$$M\_R = \rho_{M_R} V_L \tag{A21}$$

$$\rho_{M_R} = f(x) \tag{A22}$$

$$m_{out} = MAX(f_V(V_L - V_R), 0) \tag{A23}$$

$$r = f(T_R, C_i) \tag{A24}$$

$$C_i = \frac{x_i M_R}{V_L} \tag{A25}$$

$$\frac{dH_R}{dt} = -\sum_i m_{i,in} \Delta h_{i,T_{in},T_R} - \Delta h_{RXN} r + q_{HX} \tag{A26}$$

$$H_R = M_R h_R \tag{A27}$$

$$h\_R = \sum_i x_i h_{i,T_R} \tag{A28}$$

$$\Delta h_{i,T_{in},T_R} = h_{i,T_{in}} - h_{i,T_R} \tag{A29}$$

$$\Delta h_{RXN} = f(T_R) \tag{A30}$$

$$h_{i,T_{in}} = f(T_{in}) \tag{A31}$$

$$h_{i,T_R} = f(T_R) \tag{A32}$$

$$q_{HX} = f_T\left(T_R - T_{setpoint}\right) \tag{A33}$$

where:
m_{in} = the total molar flowrate of material into the reaction chamber;
m_{out} = the total molar flowrate of material out of the reaction chamber;
x_i = the liquid mole fraction of component i within the reaction chamber;
M_i = the molar inventory of component i within the reaction chamber;
M_R = the total molar inventory within the reaction chamber;
V_R = the volume of reaction chamber (f_V represents a PI function – representing level/volume control);
V_L = the volume of the reactor inventory;
T_R = temperature within the reaction chamber;
ρ_{M_R} = density of the reaction chamber inventory;
r = the volume specific molar rate of reaction, a function of T_R and C_i (i = 1,2…n);
v_i = the stoichiometric coefficient of component i in the reaction;

C_i = the concentration of component i within the reaction chamber;
H_R = the enthalpy of the reactor system;
h_R = the molar specific enthalpy of the reactor system.
h_{i,T_R} = the enthalpy of component i at T_R;
$h_{i,T_{in}}$ = the enthalpy of component i at the inlet temperature, T_{in};
$\Delta h_{i,T_{in},T_R}$ = the molar specific enthalpy change required by the reactor system to change component i from the inlet temperature to the temperature of the reactor contents;
h_{RXN} = the enthalpy of reaction (a function of T_R);
q_{HX} = the heat flux from outside the reactor system;
$T_{setpoint}$ = the setpoint temperature for the reactor (f_T represents a PI function).

The volume specific molar rates of reaction for the three reactions are modelled according to the following kinetics (Equations (A34)–(A40)):

$$r_{Bunsen} = k_1[SO_2][I_2][H_2O] \tag{A34}$$

$$r_{H_2SO_4\ Decomposition} = k_2[H_2SO_4] \tag{A35}$$

$$r_{HI\ Decomposition} = 2(k_3[HI]^2 - k_{-3}[H_2][I_2]) \tag{A36}$$

$$k_1 = A_1 exp\left(-\frac{E_1}{R}\left\{\frac{1}{T} - \frac{1}{298.15}\right\}\right) \tag{A37}$$

$$k_2 = A_2 exp\left(-\frac{E_2}{RT}\right) \tag{A38}$$

$$k_3 = A_3 exp\left(-\frac{E_3}{RT}\right) \tag{A39}$$

$$k_{-3} = A_{-3}\ exp\left(-\frac{E_{-3}}{RT}\right) \tag{A40}$$

Using absolute temperature in K, molar concentrations in mol l^{-1} and the activation energies and pre-exponential factors from [38] given in Table A1.

Table A1. HTSE steady state process parameters.

Parameter	Value	Units
E_1	4.187	kJ mol^{-1}
E_2	73.1	kJ mol^{-1}
E_3	108	kJ mol^{-1}
E_{-3}	184	kJ mol^{-1}
A_1	3×10^{-6}	$L^2\ mol^{-1}\ s^{-1}$
A_2	6.8×10^4	s^{-1}
A_3	1.596×10^7	L $mol^{-1}\ s^{-1}$
A_{-3}	1×10^{-11}	s^{-1}

References

1. Staffell, I.; Scamman, D.; Velazquez, A.; Balcombe, P.; Dodds, P.E.; Ekins, P.; Shah, N.; Ward, K.R. The Role of Hydrogen and Fuel Cells in the Global Energy System. *Energy Environ. Sci.* **2019**, *12*, 463–491. [CrossRef]
2. Fast-Tracking Nuclear Hydrogen: IAEA to Develop Roadmap for Commercial Deployment. Available online: https://www.iaea.org/newscenter/news/fast-tracking-nuclear-hydrogen-iaea-to-develop-roadmap-for-commercial-deployment (accessed on 26 March 2024).
3. Constantin, A. Nuclear Hydrogen Projects to Support Clean Energy Transition: Updates on International Initiatives and IAEA Activities. *Int. J. Hydrog. Energy* **2024**, *54*, 768–779. [CrossRef]
4. Hydrogen Production with Operating Nuclear Power Plants. Available online: https://www.iaea.org/sites/default/files/2023_h2_booklet_web.pdf (accessed on 26 April 2024).
5. Bay Hydrogen Hub—Hydrogen-4-Hanson: Department for Energy Security and Net Zero (DESNEZ) Industrial Hydrogen Accelerator Stream 2A Feasibility Study. Available online: https://assets.publishing.service.gov.uk/government/uploads/system/uploads/attachment_data/file/1161490/iha-22-edf-final-feasibility-report.pdf (accessed on 26 February 2024).
6. Hydrogen Projects Database. Available online: https://www.iea.org/data-and-statistics/data-product/hydrogen-production-and-infrastructure-projects-database (accessed on 26 April 2024).
7. Levelised Cost of Hydrogen Maps. Available online: https://www.iea.org/data-and-statistics/data-tools/levelised-cost-of-hydrogen-maps (accessed on 26 April 2024).
8. International Atomic Energy Agency. Examining the Technoeconomics of Nuclear Hydrogen Production and Benchmark Analysis of the IAEA HEEP software. IAEA TECDOC 1859, 2018.
9. Naterer, G.F.; Dincer, I.; Zamfirescu, C. *Hydrogen Production from Nuclear Energy*; Springer International Publishing AG: Midtown Manhattan, New York City, USA, 2013.
10. UK Hydrogen Strategy. Available online: https://assets.publishing.service.gov.uk/media/64c7e8bad8b1a70011b05e38/UK-Hydrogen-Strategy_web.pdf (accessed on 26 April 2024).
11. Shahabuddin, M.; Alim, M.A.; Alam, T.; Mofijur M.; Ahmed, S.F.; Perkins G.A. Critical Review on the Development and Challenges of Concentrated Solar Power Technologies. *Sustainable Energy Technol. Assess.* **2021**, *47*, 101434. [CrossRef]
12. El-Emam R.S.; Özcan, H. Comprehensive Review on the Technoeconomics of Sustainable Large-Scale Clean Hydrogen Production. *J. Cleaner Prod.* **2019**, *220*, 593–609. [CrossRef]
13. Beyond Electricity: The Economics of Nuclear Cogeneration. Available online: https://www.oecd-nea.org/jcms/pl_71699/beyond-electricity-the-economics-of-nuclear-cogeneration (accessed on 25 March 2024).
14. Gabriel, K.S.; El-Emam, R.S.; Zamfirescu, C. Technoeconomics of large-scale clean hydrogen production—A review. *Int. J. Hydrogen Energy* **2022**, *47*, 30788–30798. [CrossRef]
15. H2A: Hydrogen Analysis Production Methods. Available online: https://www.nrel.gov/hydrogen/h2a-production-models.html (accessed on 26th April 2024).
16. GEN IV International Forum. Available online: https://www.gen-4.org/gif/jcms/c_9509/tools (accessed on 26 April 2024).
17. Frick, K.; Wendt, D.; Talbot, P.; Rabiti, C.; Boardman, R. Technoeconomic Assessment of Hydrogen Cogeneration via High Temperature Steam Electrolysis with a Light-Water Reactor. *Appl. Energy* **2022**, *306*, 118044. [CrossRef]
18. Bhattacharyya, R.; Singh, K.K.; Bhanja, K.; Grover, R.B. Assessing Techno-Economic Uncertainties in Nuclear Power-to-X Processes: The Case of Nuclear Hydrogen Production via Water Electrolysis. *Int. J. hydrog. Energy* **2023**, *48*, 14149–14169. [CrossRef]
19. Epiney, A.; Rabiti, C.; Talbot, P.; Alfonsi, A. Economic Analysis of a Nuclear Hybrid Energy System in a Stochastic Environment including Wind Turbines in an Electricity Grid. *Appl. Energy* **2020**, *260*, 114227. [CrossRef]
20. Antony, A.; Maheshwari, N.K.; Rama Rao, A. A Generic Methodology to Evaluate Economics of Hydrogen Production Using Energy from Nuclear Power Plants. *Int. J. Hydrog. Energy* **2017**, *42*, 25813–25823. [CrossRef]
21. Slavin, B.; Wang, R.; Roy, D.; Ling-Chin, J.; Roskilly, A.P. Techno-Economic Analysis of Direct Air Carbon Capture and Hydrogen Production Integrated with a Small Modular Reactor. *Appl. Energy* **2024**, *356*, 122407. [CrossRef]
22. IEAGHG Technical Report, "Techno-Economic Evaluation of SMR Based Standalone (Merchant) Hydrogen Plant with CCS", February **2017**. Available online: https://ieaghg.org/exco_docs/2017-02.pdf (accessed on 29 April 2024).
23. El-Emam, R.S.; Khamis, I. International Collaboration in the IAEA Nuclear Hydrogen Production Program for Benchmarking of HEEP. *Int. J. Hydrog. Energy* **2016**, *42*, 3566–3571. [CrossRef]
24. Khamis, I.; Malshe, U.D. HEEP: A new tool for the economic evaluation of hydrogen economy. *Int. J. Hydrog. Energy* **2010**, *35*, 8398–8406. [CrossRef]
25. El-Emam, R.S.; Ozcan, H.; Dincer, I. Comparative Cost Evaluation of Nuclear Hydrogen Production Methods with the Hydrogen Economy Evaluation Program (HEEP). *Int. J. Hydrog. Energy* **2015**, *40*, 11168–11177. [CrossRef]

26. Lovering, J.R.; Yip, A.; Nordhaus, T. Historical construction costs of global nuclear power reactors. *Energy Policy* **2016**, *91*, 371–382. [CrossRef]
27. Hydrogen Production Costs. Available online: https://www.gov.uk/government/publications/hydrogen-production-costs-2021 (accessed on 26 April 2024).
28. Civil Nuclear: Roadmap to 2050. Available online: https://assets.publishing.service.gov.uk/media/65c0e7cac43191000d1a457d/6.8610_DESNZ_Civil_Nuclear_Roadmap_report_Final_Web.pdf (accessed on 26 April 2024).
29. Perfiliev, M.V. Problems of High Temperature Electrolysis of Water Vapour. *Int. J. Hydrog. Energy* **1994**, *19*. 227–230. [CrossRef]
30. Ni, M.; Leung, M.K.H.; Leung, D.Y.C. An Electrochemical Model of a Solid Oxide Steam Electrolyser for Hydrogen Production. *Chem. Eng. Tech.* **2006**, *29*, 636–642. [CrossRef]
31. Ferguson, J.R.; Fiard, J.M.; Herbin, R. Three-dimensional numerical simulation for various geometries of solid oxide fuel cells. *Power Sources* **1996**, *58*, 109–122. [CrossRef]
32. Solid Oxide Electrolysis System Demonstration. Available online: https://www.hydrogen.energy.gov/docs/hydrogenprogramlibraries/pdfs/review23/ta039_ghezel-ayagh_2023_o-pdf.pdf (accessed on 26 April 2024).
33. Offshore Wind and Hydrogen: Solving the Integration Challenge. Available online: https://ore.catapult.org.uk/wp-content/uploads/2020/09/Solving-the-Integration-Challenge-ORE-Catapultr.pdf (accessed on 26 April 2024).
34. HyNet Low Carbon Hydrogen Plant. Available online: https://assets.publishing.service.gov.uk/media/5e4ac453ed915d4fff2dbf04/HS384_-_Progressive_Energy_-_HyNet_hydrogen.pdf (accessed on 26 April 2024).
35. Wang, L.J.; Zhang, P.; Chen, S.Z.; Xu, J.M. Overview of the Development of Catalysts for HI Decomposition in the Iodine-Sulfur Thermochemical Cycle at INET. *Nucl. Eng. Des.* **2014**, *271*, 60–63. [CrossRef]
36. Zhang, K.; Bao, W.; Chang, L.; Wang, H. A Review of Recent Researches on Bunsen Reaction for Hydrogen Production via S–I Water and H_2S Splitting Cycles. *J. Energy Chem.* **2019**, *33*, 46–58. [CrossRef]
37. Preliminary Economic Assessment of GW Scale Nuclear Enabled Hydrogen Production. Available online: https://www.nnl.co.uk/wp-content/uploads/2022/03/Preliminary-Economic-Assessment-of-Nuclear-Enabled-Hydrogen-Production-Final-Approved.pdf (accessed on 26 April 2024).
38. Brown, N.R.; Oh, S; Revankar, S.T; Vierow, K; Rodriguez, S.; Cole, R.; Gauntt, R. Simulation of Sulfur-Iodine Thermochemical Hydrogen Production Plant Coupled to High-Temperature Heat Source. *Nucl. Technol.* **2009**, *167*, 95–106. [CrossRef]